



**HAL**  
open science

## Sensitivity analysis of the elasto-geometrical model of cable-driven parallel robots

Sana Baklouti, Stéphane Caro, Eric Courteille

► **To cite this version:**

Sana Baklouti, Stéphane Caro, Eric Courteille. Sensitivity analysis of the elasto-geometrical model of cable-driven parallel robots. 3rd International Conference on Cable-Driven Parallel Robots, CableCon 2017, Aug 2017, Quebec City, Canada. 10.1007/978-3-319-61431-1\_4 . hal-01619371

**HAL Id: hal-01619371**

**<https://univ-rennes.hal.science/hal-01619371v1>**

Submitted on 11 Dec 2019

**HAL** is a multi-disciplinary open access archive for the deposit and dissemination of scientific research documents, whether they are published or not. The documents may come from teaching and research institutions in France or abroad, or from public or private research centers.

L'archive ouverte pluridisciplinaire **HAL**, est destinée au dépôt et à la diffusion de documents scientifiques de niveau recherche, publiés ou non, émanant des établissements d'enseignement et de recherche français ou étrangers, des laboratoires publics ou privés.

# Sensitivity Analysis of the Elasto-Geometrical Model of Cable-Driven Parallel Robots

Sana Baklouti, Stéphane Caro and Eric Courteille

**Abstract** This paper deals with the sensitivity analysis of the elasto-geometrical model of Cable-Driven Parallel Robots (CDPRs) to their geometric and mechanical uncertainties. This sensitivity analysis is crucial in order to come up with a robust model-based control of CDPRs. Here, 62 geometrical and mechanical error sources are considered to investigate their effect onto the static deflection of the moving-platform (MP) under an external load. A reconfigurable CDPR, named "CAROCA", is analyzed as a case of study to highlight the main uncertainties affecting the static deflection of its MP.

## 1 Introduction

In recent years, there has been an increasing number of research works on the subject of Cable-Driven Parallel Robots (CDPRs). The latter are very promising for engineering applications due to peculiar characteristics such as large workspace, simple structure and large payload capacity. For instance, CDPRs have been used in many applications like rehabilitation [1], pick-and-place [2], sandblasting and painting [4, 3] operations.

Many spatial prototypes are equipped with eight cables for six Degrees of Freedom (DOF) such as the CAROCA prototype, which is the subject of this paper.

---

Sana Baklouti  
Université Bretagne-Loire, INSA-LGCGM-EA 3913, 20, avenue des Buttes de Cöesmes, 35043  
Rennes, France, e-mail: sana.baklouti@insa-rennes.fr

Stéphane Caro  
CNRS, Laboratoire des Sciences du Numérique de Nantes, UMR CNRS n6004, 1, rue de la Noë,  
44321 Nantes, France, e-mail: stephane.caro@ls2n.fr

Eric Courteille  
Université Bretagne-Loire, INSA-LGCGM-EA 3913, 20, avenue des Buttes de Cöesmes, 35043  
Rennes, France, e-mail: eric.courteille@insa-rennes.fr

To customize CDPRs to their applications and enhance their performances, it is necessary to model, identify and compensate all the sources of errors that affect their accuracy.

Improving accuracy is still possible once the robot is operational through a suitable control scheme. Numerous control schemes were proposed to enhance the CDPRs precision on static tasks or on trajectory tracking [5, 6, 7]. The control can be either off-line through external sensing in the feedback signal [2], or on-line control based on a reference model [8].

This paper focuses on the sensitivity analysis of the CDPR MP static deflection to uncertain geometrical and mechanical parameters. As an illustrative example,



Fig. 1: CAROCA prototype: a reconfigurable CDPR (Courtesy of IRT Jules Verne, Nantes)

a suspended configuration of the reconfigurable CAROCA prototype, shown in Fig. 1, is studied. First, the manipulator under study is described. Then, its elasto-geometrical model is written while considering cable mass and elasticity in order to express the static deflection of the MP subjected to an external load. An exhaustive list of geometrical and mechanical uncertainties is given. Finally, the sensitivity of the MP static deflection to these uncertainties is analyzed.

## 2 Parametrization of the CAROCA prototype

The reconfigurable CAROCA prototype illustrated in Fig. 1 was developed at IRT Jules Verne for industrial operations in cluttered environment such as painting and sandblasting large structures [3, 4]. This prototype is reconfigurable because its pulleys can be displaced in a discrete manner on its frame. The size of the latter is 7 m long, 4 m wide and 3 m high. The rotation-resistant steel cables Carl Stahl Technocables Ref 1692 of the CAROCA prototype are 4 mm diameter. Each cable consists of 18 strands twisted around a steel core. Each strand is made up of 7 steel

wires. The cable breaking force is 10.29 kN.  $\rho$  denotes the cable linear mass and  $E$  the cable modulus of elasticity.

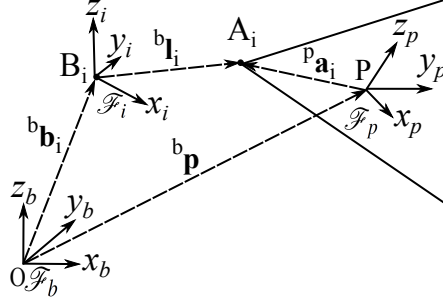


Fig. 2: The  $i$ th closed-loop of a CDPR

As shown in Fig. 2, the Cartesian coordinate vectors of anchor points  $A_i$  and exit points  $B_i$  are denoted  $\mathbf{a}_i$  and  $\mathbf{b}_i$ . Vector  $\mathbf{p}$  represents the Cartesian coordinates of the MP geometric center,  $P$ , expressed in  $\mathcal{F}_b = \{O, x_b, y_b, z_b\}$ . The Cartesian coordinates of  $A_i$  ( $B_i$ , resp.) expressed in the MP frame  $\mathcal{F}_p = \{P, x_p, y_p, z_p\}$  (in the base frame  $\mathcal{F}_b$ , resp.) are given in Tab. 1. The cable frame  $\mathcal{F}_i = \{B_i, x_i, y_i, z_i\}$  is associated to the  $i$ th cable, where axes  $z_i$  and  $z_b$  are parallel.

Table 1: Cartesian coordinates of anchor points  $A_i$  (exit points  $B_i$ , resp.) expressed in  $\mathcal{F}_p$  (in  $\mathcal{F}_b$ , resp.)

	x (m)	y (m)	z (m)		x (m)	y (m)	z (m)
$B_1$	-3.5	2	3.5	$A_1$	0.2	0.15	0.125
$B_2$	3.5	2	3.5	$A_2$	-0.2	0.15	-0.125
$B_3$	-3.5	2	3.5	$A_3$	-0.2	-0.15	-0.125
$B_4$	3.5	2	3.5	$A_4$	0.2	-0.15	0.125
$B_5$	-3.5	-2	3.5	$A_5$	-0.2	0.15	0.125
$B_6$	3.5	-2	3.5	$A_6$	0.2	0.15	-0.125
$B_7$	-3.5	-2	3.5	$A_7$	0.2	-0.15	-0.125
$B_8$	3.5	-2	3.5	$A_8$	-0.2	-0.15	0.125

### 3 Elasto-geometric modeling

In this section, both sag-introduced and axial stiffness of cables are considered in the elasto-geometrical modeling of CDPR. The inverse elasto-geometrical model and the direct elasto-geometrical model of CDPR are presented. Then, the variations in static deflection due to external loading is defined as a sensitivity index.

#### 3.1 Inverse Elasto-Geometric Modeling (IEGM)

The IEGM of a CDPR aims at calculating the unstrained cable length for a given pose of its MP. If both cable mass and elasticity are considered, the inverse kinematics of the CDPR and its static equilibrium equations should be solved simultaneously. The

IEGM is based on geometric closed loop equations, cable sagging relationships and static equilibrium equations.

The geometric closed-loop equations take the form:

$${}^b\mathbf{p} = {}^b\mathbf{b}_i + {}^b\mathbf{l}_i - {}^b\mathbf{R}_p {}^p\mathbf{a}_i, \quad (1)$$

where  ${}^b\mathbf{R}_p$  is the rotation matrix from  $\mathcal{F}_b$  to  $\mathcal{F}_p$  and  $\mathbf{l}_i$  is the cable length vector. The cable sagging relationships between the forces  ${}^i\mathbf{f}_i = [{}^i f_{xi}, 0, {}^i f_{zi}]$  applied at the end point  $A_i$  of the  $i$ th cable and the coordinates vector  ${}^i\mathbf{a}_i = [{}^i x_{Ai}, 0, {}^i z_{Ai}]$  of the same point resulting from the sagging cable model [9] are expressed in  $\mathcal{F}_i$  as follows:

$${}^i x_{Ai} = \frac{{}^i f_{xi} L_{usi}}{ES} + \frac{|{}^i f_{xi}|}{\rho g} \left[ \sinh^{-1} \left( \frac{{}^i f_{zi}}{f_{xi}^c} \right) - \sinh^{-1} \left( \frac{{}^i f_{zi} - \rho g L_{usi}}{{}^i f_{xi}} \right) \right], \quad (2a)$$

$${}^i z_{Ai} = \frac{{}^i f_{xi} L_{usi}}{ES} - \frac{\rho g L_{usi}^2}{2ES} + \frac{1}{\rho g} \left[ \sqrt{{}^i f_{xi}^2 + {}^i f_{zi}^2} - \sqrt{{}^i f_{xi}^2 + ({}^i f_{zi} - \rho g L_{usi})^2} \right], \quad (2b)$$

where  $L_{usi}$  is the unstrained length of  $i$ th cable,  $g$  is the acceleration due to gravity,  $S$  is the cross sectional area of the cables.

The static equilibrium equations of the MP are expressed as:

$$\mathbf{W}\mathbf{t} + \mathbf{w}_{ex} = 0, \quad (3)$$

where  $\mathbf{W}$  is the wrench matrix,  $\mathbf{w}_{ex}$  is the external wrench vector and  $\mathbf{t}$  is the 8-dimensional cable tension vector. Those tensions are computed based on the tension distribution algorithm described in [10].

### 3.2 Direct elasto-geometrical model (DEGM)

The direct elasto-geometrical model (DEGM) aims to determine the pose of the mobile platform for a given set of unstrained cable lengths. The constraints of the DEGM are the same as the IEGM, i.e. Eq. (1) to Eq. (3). If the effect of cable weight on the static cable profile is non-negligible, the direct kinematic model of CDPRs will be coupled with the static equilibrium of the MP. For a 6 DOFs CDPR with 8 driving cables, there are 22 equations and 22 unknowns. In this paper, the non-linear Matlab function “*lsqnonlin*” is used to solve the DEGM.

### 3.3 Static deflection

If the compliant displacement of the MP under the external load is small, the static deflection of the MP can be calculated by its static Cartesian stiffness matrix [11]. However, once the cable mass is considered, the sag-introduced stiffness should be taken into account. Here, the small compliant displacement assumption is no longer valid, mainly for heavy or/and long cables with light mobile platform. Consequently, the static deflection can not be calculated through the Cartesian stiffness matrix. In this paper, the IEGM and DEGM are used to define and calculate the static deflection of the MP under an external load. The CDPR stiffness is characterized by the static deflection of the MP. Note that only the positioning static deflection of the MP is considered in order to avoid the homogenization problem [12].

As this paper deals with the sensitivity of the CDPR accuracy to all geometrical and mechanical errors, the elastic deformations of the CDPR is involved. This problem is solved by deriving the static deflection of the CDPR obtained by the subtraction of the poses calculated with and without an external payload. For a desired pose of the MP, the IEGM gives a set of unstrained cable lengths  $\mathbf{L}_{us}$ . This set is used by the DEGM to calculate first, the pose of the MP under its own weight. Then, the pose of the MP is calculated when an external load (mass addition) is applied. Therefore, the static deflection of the MP is expressed as:

$$\mathbf{dp}_{j,k} = \mathbf{p}_{j,k} - \mathbf{p}_{j,1}, \quad (4)$$

where  $\mathbf{p}_{j,1}$  is the pose of the MP considering only its own weight for the  $j^{th}$  pose configuration and  $\mathbf{p}_{j,k}$  is the pose of the MP for the set of the  $j^{th}$  pose and  $k^{th}$  load configuration.

## 4 Error modeling

This section aims to define the error model of the elasto-geometrical CDPR model. Two types of errors are considered: geometrical errors and mechanical errors.

### 4.1 Geometrical errors

The geometrical errors of the CDPR are described by  $\delta\mathbf{b}_i$ , the variation in vector  $\mathbf{b}_i$ ,  $\delta\mathbf{a}_i$ , the variation in vector  $\mathbf{a}_i$ , and  $\delta\mathbf{g}$ , the uncertainty vector of the gravity center position; So, 51 uncertainties. The geometric errors can be divided into base frame geometrical errors and MP geometrical errors and mainly due to manufacturing errors.

#### 4.1.1 Base frame geometrical errors

The base frame geometrical errors are described by vectors  $\delta\mathbf{b}_i$ , ( $i=1..8$ ). As the point  $B_i$  is considered as part of its correspondent pulley, it is influenced by the elasticity of the pulley mounting and its assembly tolerance.  $\mathbf{b}_i$  is particularly influenced by pulleys tolerances and reconfigurability impact.

#### 4.1.2 Moving-platform geometrical errors

The MP geometrical errors are described by vectors  $\delta\mathbf{a}_i$ , ( $i=1..8$ ), and  $\delta\mathbf{g}$ . The gravity center of the MP is often supposed to coincide with its geometrical center  $P$ . This hypothesis means that the moments generated by an inaccurate knowledge of the gravity center position or by its potential displacement are neglected. The Cartesian coordinate vector of the geometric center  $G$  does not change in frame  $\mathcal{F}_p$ , but strongly depends on the real coordinates of exit points  $A_i$  that are related to uncertainties in mechanical welding of the hooks and in MP assembly.

### 4.2 Mechanical errors

The mechanical errors of the CDPR are described by the uncertainty in the MP mass ( $\delta m$ ) and the uncertainty on the cables mechanical parameters ( $\delta\rho$  and  $\delta E$ ).

Besides, uncertainties in the cables tension  $\delta \mathbf{t}$  affect the error model. As a result, 11 mechanical error sources are taken into account.

#### 4.2.1 End-effector mass

As the MP is a mechanically welded structure, there may be some differences between the MP mass and inertia matrix given by the CAD software and the real ones. The MP mass and inertia may also vary in operation. In this paper, MP mass uncertainty  $\delta m$  is about  $\pm 10\%$  the nominal mass.

#### 4.2.2 Cables parameters

*Linear mass:* The linear mass  $\rho$  of CAROCA cables is equal to 0.1015 kg/m. The uncertainty of this parameter can be calculated from the measurement procedure as:  $\delta \rho = \frac{m_c \delta L + L \delta m_c}{L^2}$ , where  $m_c$  is the measured cable mass for a cable length  $L$ .  $\delta L$  and  $\delta m_c$  are respectively the measurement errors of the cable length and mass.

*Modulus of elasticity:* This paper uses experimental hysteresis loop to discuss the modulus of elasticity uncertainty. Figure 3 shows the measured hysteresis loop of the 4 mm cable where the unloading path does not correspond to the loading path. The area in the center of the hysteresis loop is the energy dissipated due to internal friction in the cable. It depicts a non-linear correlation in the lower area between load and elongation.

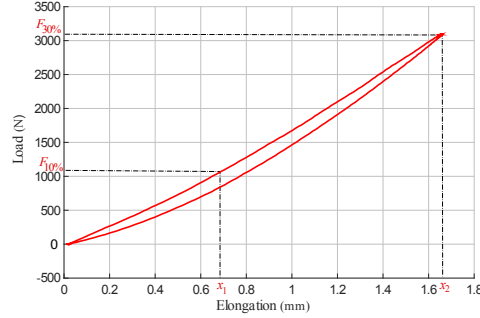


Fig. 3: Load-elongation diagram of a steel wire cable measured in steady state conditions at the rate of 0.05 mm/s

Based on experimental data presented in Fig. 3, Table 2 presents the modulus of elasticity of a steel wire cable for different operating margins, when the cable is in loading or unloading phase. This modulus is calculated as follows:

$$E_{p-q} = L_c \frac{F_{q\%} - F_{p\%}}{S(x_q - x_p)}, \quad (5)$$

where  $S$  is the metallic cross-sectional area, i.e. the value obtained from the sum of the metallic cross-sectional areas of the individual wires in the rope based on their

nominal diameters.  $x_p$  and  $x_q$  are the elongations at forces equivalent to  $p\%$  and  $q\%$  ( $F_{p\%}$  and  $F_{q\%}$ ), respectively, of the nominal breaking force of the cable measured during the loading path (Fig. 3).  $L_c$  is the measured initial cable length.

Table 2: Modulus of elasticity while loading or unloading phase

Modulus of elasticity (GPa)	$E_{1-5}$	$E_{5-10}$	$E_{5-20}$	$E_{5-30}$	$E_{10-15}$	$E_{10-20}$	$E_{10-30}$	$E_{20-30}$
Loading	72.5	83.2	92.7	97.2	94.8	98.3	102.2	104.9
Unloading	59.1	82.3	96.2	106.5	100.1	105.1	115	126.8

For a given range of loads (Tab. 2), the uncertainty on the modulus of elasticity depends only on the corresponding elongations and tensions measurements. In this case, the absolute uncertainty associated with applied force and resulting elongation measurements from the test bench outputs is estimated to be  $\pm 1$  N and  $\pm 0.03$  mm, respectively; so, an uncertainty of  $\pm 2$  GPa can be applied to the calculation of the modulus of elasticity.

According to the International Standard ISO 12076, the modulus of elasticity of a steel wire cable is  $E_{10-30}$ . However, the CDPR cables do not work always between  $F_{10\%}$  and  $F_{30\%}$  in real life and the cables can be in loading or unloading phase. The mechanical behavior of cables depends on MP dynamics, which affects the variations in cable elongations and tensions. From Table 2, it is apparent that the elasticity moduli of cables change with the operating point changes. For the same applied force, the modulus of elasticity for loaded and unloaded cables are not the same. While the range of the MP loading is unknown, a large range of uncertainties on the modulus of elasticity should be defined as a function of the cable tensions.

#### 4.2.3 Tension distribution

Two cases of uncertainties of force determination can be defined depending on the control scheme:

The first case is when the control scheme gives a tension set-point to the actuators resulting from the force distribution algorithm. If there is no feedback about the tensions measures, the range of uncertainty is relatively high. Generally, the effort of compensation does not consider dry and viscous friction in cable drum and pulleys. This non-compensation leads to static errors and delay [13] that degrade the CDPR control performance. That leads to a large range of uncertainties in tensions. As the benefit of tension distribution algorithm used is less important in case of a suspended configuration of CDPR than the fully-constrained one [14], a range of  $\pm 15$  N is defined.

The second case is when the tensions are measured. If measurement signals are very noisy, amplitude peaks of the correction signal may lead to a failure of the force distribution. Such a failure may also occur due to variations in the MP and pulleys parameters. Here, the deviation is defined based on the measurement tool precision. However, it remains lower than the deviation of the first case by at least 50%.



## 5 Sensitivity Analysis

Due to the non-linearities of the elasto-geometrical model, explicit sensitivity matrix and coefficients [15, 16] cannot be computed. Therefore, the sensitivity of the elasto-geometrical model of the CDPR to geometrical and mechanical errors is evaluated statistically. Here, MATLAB has been coupled with modeFRONTIER, a process integration and optimization software platform [17] for the analysis.

The RMS (Root Mean Square) of the static deflection of CAROCA MP is studied. The nominal mass of the MP and the additional mass are equal to 180 kg and 50 kg, respectively.

### 5.1 Influence of mechanical errors

In this section, all the uncertain parameters of the elasto-geometrical CAROCA model are defined with uniformly distributed deviations. The uncertainty range and discretization step are given in Tab. 3. In this basis, 2000 SOBOL quasi-randm observations are created.

Table 3: Uncertainties and steps used to design the error model

Parameter	$m$ (kg)	$\rho$ (kg/m)	$E$ (GPa)	$a_i$ (m)	$b_i$ (m)	$\delta t_i$ (N)
Uncertainty range	$\pm 18$	$\pm 0.01015$	$\pm 18$	$\pm 0.015$	$\pm 0.03$	$\pm 15$
Step	0.05	$3 \cdot 10^{-5}$	0.05	0.0006	0.0012	0.1

In this configuration, the operating point of the MP is supposed to be unknown. A large variation range of the modulus of elasticity is considered. The additional mass corresponds to a variation in cable tensions from 574 N to 730 N, which corresponds to a modulus of elasticity of 84.64 GPa. Thus, while the operating point of the MP is unknown, an uncertainty of  $\pm 18$  GPa is defined with regard to the measured modulus of elasticity  $E = 102$  GPa.

Figure 4a displays the distribution fitting of the static deflection RMS. It shows that the RMS distribution follows a quasi-uniform law whose mean  $\mu_1$  is equal to 1.34 mm. The RMS of the static deflection of the MP is bounded between a minimum value  $RMS_{min}$  equal to 1.12 mm and a maximum value  $RMS_{max}$  equal to 1.63 mm; a variation of 0.51 mm under all uncertainties, which presents 38% of the nominal value of the static deflection.

Figure 4b depicts the RMS of the MP static deflection as a function of variations in  $E$  and  $\rho$  simultaneously, whose values vary respectively from 0.09135 to 0.11165 kg/m and from 84.2 to 120.2 GPa. The static deflection is very sensitive to cables mechanical behavior. The RMS varies from 0.42 mm to 0.67 mm due to the uncertainties of these two parameters only. As a matter of fact, the higher the cable modulus of elasticity, the smaller the RMS of the MP static deflection. Conversely, the smaller the linear mass of the cable, the smaller the RMS of the MP static deflection. Accordingly, the higher the sag-introduced stiffness, the higher the MP static deflection. Besides, the higher the axial stiffness of the cable, the lower the MP static deflection.

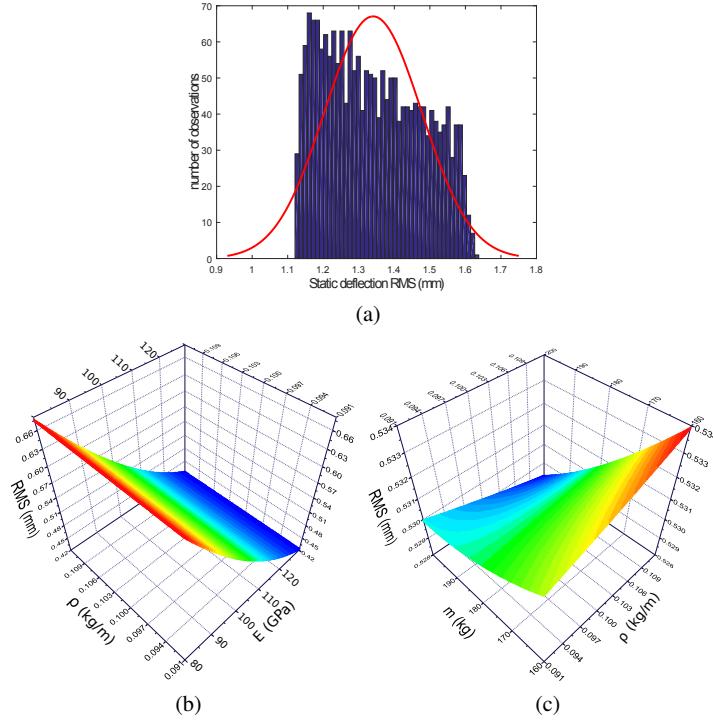


Fig. 4: (a) Distribution of the RMS of the MP static deflection (b) Evolution of the RMS under a simultaneous variations of  $E$  and  $\rho$  (c) Evolution of the RMS under a simultaneous variations of  $m$  and  $\rho$

Figure 4c illustrates the RMS of the MP static deflection as a function of variations in  $\rho$  and  $m$ , whose value varies from 162 kg to 198 kg. The RMS varies from 0.52 mm to 0.53 mm due to the uncertainties of these two parameters only. The MP mass affects the mechanical behavior of cables: the heavier the MP, the larger the axial stiffness, the smaller the MP static deflection. Therefore, a fine identification of  $m$  and  $\rho$  is very important to establish a good CDPR model.

Comparing to the results plotted in Fig. 4b, it is clear that  $E$  affects the RMS of the MP static deflection more than  $m$  and  $\rho$ . As a conclusion, the integration of cables hysteresis effects on the error model is necessary and improves force algorithms and the identification of the robot geometrical parameters [16].

## 5.2 Influence of geometrical errors

In this section, the cable tension set-points during MP operation are supposed to be known; so, the modulus of elasticity can be calculated around the operating point and the confidence interval is reduced to  $\pm 2$  GPa. The uncertainty range and the discretization step are provided in Tab. 4.

Table 4: Uncertainties and steps used to design the error model

Parameter	$m$ (kg)	$\rho$ (kg/m)	$E$ (GPa)	$\mathbf{a}_i$ (m)	$\mathbf{b}_i$ (m)	$\delta t_i$ (N)
Uncertainty range	$\pm 18$	$\pm 0.01015$	$\pm 2$	$\pm 0.015$	$\pm 0.03$	$\pm 15$
Step	0.05	$3*10^{-5}$	0.05	0.0006	0.0012	0.1

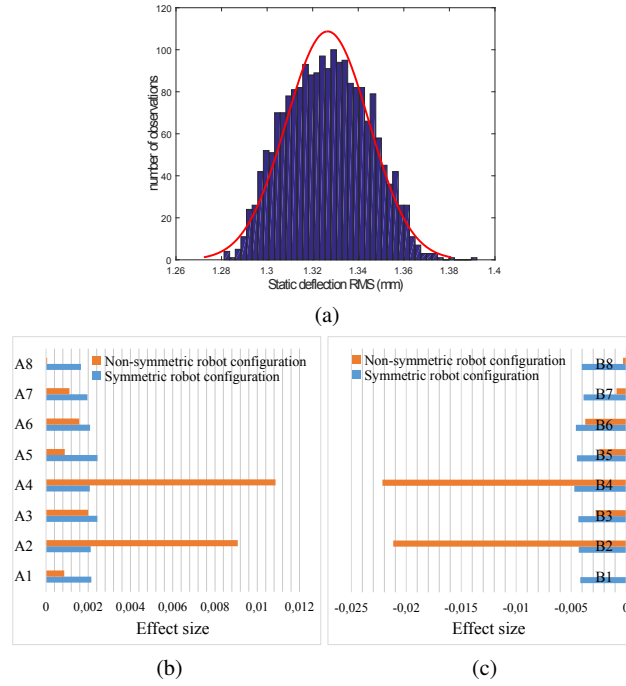


Fig. 5: (a) Distribution of the RMS of the MP static deflection (b) Effect of uncertainties in  $\mathbf{a}_i$  (c) Effect of uncertainties in  $\mathbf{b}_i$

Figure 5a displays the distribution fitting of the MP static deflection RMS. It shows that the RMS distribution follows a normal law whose mean  $\mu_2$  is equal to 1.32 mm and its standard deviation  $\sigma_2$  is equal to 0.01 mm. This deviation is relatively small, which allows to say that the calibration through static deflection is not obvious. The RMS of the static deflection of the MP is bounded between a minimum value  $RMS_{min}$  equal to 1.28 mm and a maximum value  $RMS_{max}$  equal to 1.39 mm; a variation of 0.11 mm under all uncertainties. The modulus of elasticity affects the static compliant of the MP, which imposes to always consider  $E$  error while designing a CDPR model.

The bar charts plotted in Fig. 5b and Fig. 5c present, respectively, the effects of the uncertainties in  $\mathbf{a}_i$  and  $\mathbf{b}_i$ , ( $i=1..8$ ), to the static deflection of the CAROCA for symmetric (0 m, 0 m, 1.75 m) and non-symmetric (3.2 m, 1.7 m, 3 m) robot configurations. These effects are determined based on  $t$ -student index of each uncertain

parameter. This index is a statistical tool that can estimate the relationships between outputs and uncertain inputs. The t-Student test compares the difference between the means of two samples of designs taken randomly in the design space:

- $M_+$  is the mean of the  $n_+$  values for an objective S in the upper part of domain of the input variable,
- $M_-$  is the mean of the  $n_-$  values for an objective S in the lower part of domain of the input variable.

The  $t$ -Student is defined as  $t = \frac{|M_- - M_+|}{\sqrt{\frac{V_g^2}{n_-} + \frac{V_g^2}{n_+}}}$ , where  $V_g$  is the general variance [18].

When the MP is in a symmetric configuration, all attachment points have nearly the same effect size. However, when it is located close to points  $B_2$  and  $B_4$ , the effect size of their uncertainties becomes high. Moreover, the effect of the corresponding mobile points ( $A_2$  and  $A_4$ ) increases. It means that the closer the MP to a given point, the higher the effect of the variations in the Cartesian coordinates of the corresponding exit point of the MP onto its static deflection. That can be explained by the fact that when some cables are longer than others and become slack for a non-symmetric position, the sag effect increases. Consequently, a good identification of geometrical parameters is highly required. In order to minimize these uncertainties, a good calibration leads to a better error model.

## 6 Conclusion

This paper dealt with the sensitivity analysis of the elasto-geometrical model of CDPRs to mechanical and geometrical uncertainties. The CAROCA prototype was used as a case of study. The validity and identifiability of the proposed model are verified for the purpose of CDPR model-based control. That revealed the importance of integrating cables hysteresis effect into the error modeling to enhance the knowledge about cables mechanical behavior, especially when there is no feedback about tension measurement. It appears that the effect of geometrical errors onto the static deflection of the moving-platform is significant too. Some calibration [19, 20] and self-calibration [21, 22] approaches were proposed to enhance the CDPR performances. More efficient strategies for CDPR calibration will be performed while considering more sources of errors in a future work.

## References

1. Merlet, J. P. (2010). MARIONET, a family of modular wire-driven parallel robots. In *Advances in Robot Kinematics: Motion in Man and Machine* (pp. 53-61). Springer Netherlands.
2. Dallej, T., Gouttefarde, M., Andreff, N., Michelin, M., Martinet, P. (2011, September). Towards vision-based control of cable-driven parallel robots. In *Intelligent Robots and Systems (IROS), 2011 IEEE/RSJ International Conference on* (pp. 2855-2860). IEEE.
3. Gagliardini, L., Caro, S., Gouttefarde, M., Girin, A. (2015, May). A reconfiguration strategy for reconfigurable cable-driven parallel robots. In *Robotics and Automation (ICRA), 2015 IEEE International Conference on* (pp. 1613-1620). IEEE.
4. Gagliardini, L., Caro, S., Gouttefarde, M., Girin, A. (2016). Discrete reconfiguration planning for cable-driven parallel robots. *Mechanism and Machine Theory*, 100, 313-337.

5. Jamshidifar, H., Fidan, B., Gungor, G., Khajepour, A. (2015). Adaptive Vibration Control of a Flexible Cable Driven Parallel Robot. *IFAC-PapersOnLine*, 48(3), 1302-1307.
6. Fang, S., Frantza, D., Torlo, M., Bekes, F., Hiller, M. (2004). Motion control of a tendon-based parallel manipulator using optimal tension distribution. *IEEE/ASME Transactions On Mechatronics*, 9(3), 561-568.
7. Zi, B., Duan, B. Y., Du, J. L., Bao, H. (2008). Dynamic modeling and active control of a cable-suspended parallel robot. *Mechatronics*, 18(1), 1-12.
8. Pott, A., Mtherich, H., Kraus, W., Schmidt, V., Miermeister, P., Verl, A. (2013). IPAnema: a family of cable-driven parallel robots for industrial applications. In *Cable-Driven Parallel Robots* (pp. 119-134). Springer Berlin Heidelberg.
9. Irvine, H. M. (1992). *Cable structures*. Dover Publications.
10. Mikelsons, L., Bruckmann, T., Hiller, M., Schramm, D. (2008, May). A real-time capable force calculation algorithm for redundant tendon-based parallel manipulators. In *Robotics and Automation, 2008. ICRA 2008. IEEE International Conference on* (pp. 3869-3874). IEEE.
11. Carbone, G. (2011). Stiffness analysis and experimental validation of robotic systems. *Frontiers of Mechanical Engineering*, 6(2), 182-196.
12. Nguyen, D. Q., Gouttefarde, M. (2014). Stiffness Matrix of 6-DOF Cable-Driven Parallel Robots and Its Homogenization. In *Advances in Robot Kinematics* (pp. 181-191). Springer International Publishing.
13. De Wit, C. C., Seront, V. (1990, May). Robust adaptive friction compensation. In *Robotics and Automation, 1990. Proceedings., 1990 IEEE International Conference on* (pp. 1383-1388). IEEE.
14. Lamaury, J. (2013). Contribution a la commande des robots parallles a cbles redondance d'actionnement (Doctoral dissertation, Universit Montpellier II-Sciences et Techniques du Languedoc).
15. Zi, B., Ding, H., Wu, X., Kecskemthy, A. (2014). Error modeling and sensitivity analysis of a hybrid-driven based cable parallel manipulator. *Precision Engineering*, 38(1), 197-211.
16. Miermeister, P., Kraus, W., Lan, T., Pott, A. (2015). An elastic cable model for cable-driven parallel robots including hysteresis effects. In *Cable-Driven Parallel Robots* (pp. 17-28). Springer International Publishing.
17. modeFRONTIER, [www.esteco.com](http://www.esteco.com)
18. Courteille, E., Deblaise, D., Maurine, P. (2009, October). Design optimization of a delta-like parallel robot through global stiffness performance evaluation. In *Intelligent Robots and Systems, 2009. IROS 2009. IEEE/RSJ International Conference on* (pp. 5159-5166). IEEE.
19. dit Sandretto, J. A., Trombettoni, G., Daney, D., Chabert, G. (2014). Certified calibration of a cable-driven robot using interval contractor programming. In *Computational Kinematics* (pp. 209-217). Springer Netherlands.
20. Joshi, S. A., Surianarayan, A. (2003). Calibration of a 6-DOF cable robot using two inclinometers. *Performance metrics for intelligent systems*, 3660-3665.
21. Miermeister, P., Pott, A., Verl, A. (2012, May). Auto-calibration method for overconstrained cable-driven parallel robots. In *Robotics; Proceedings of ROBOTIK 2012; 7th German Conference on* (pp. 1-6). VDE.
22. Borgstrom, P. H., Jordan, B. L., Borgstrom, B. J., Stealey, M. J., Sukhatme, G. S., Batalin, M. A., Kaiser, W. J. (2009). Nims-pl: A cable-driven robot with self-calibration capabilities. *IEEE Transactions on Robotics*, 25(5), 1005-1015.